Available online at www.sciencedirect.com
SCIENCE DIRECT®
Advances in Space Research 35 (2005) 1925–1932
ADVANCES IN SPACE RESEARCH (a COSPAR publication)
www.elsevier.com/locate/asr

Seasonal variation of gravity wave sources from satellite observation

J.H. Jiang [a,*], S.D. Eckermann [b], D.L. Wu [a], K. Hocke [c], B. Wang [d], J. Ma [b], Y. Zhang [d]

[a] Jet Propulsion Laboratory, California Institute of Technology, Pasadena, CA, USA
[b] E.O. Hulburt Center for Space Research, Naval Research Laboratory, Washington, DC, USA
[c] National Institute of Information and Communications Technology, Japan
[d] School of Ocean and Earth Science and Technology, University of Hawaii, Honolulu, Hawaii, USA

Received 8 September 2004; received in revised form 24 January 2005; accepted 25 January 2005

Abstract

Recent high-resolution satellite observations of gravity waves in the middle atmosphere have shown correlations with the strength of the stratospheric jet stream, surface topography, and tropical convection. Seasonal variations of wave-induced stratospheric radiance variances are often the manifestations of modulations of these sources and refractive influences. In this paper, we focus on the seasonal climatology of gravity waves observed by the UARS MLS, while also showing some new results from GPS and AMSU instruments. Our analysis is aided by MWFM modeling of mountain waves at high latitudes and CMAP precipitation indices in the subtropics to provide a clearer picture of global gravity wave dynamics.

1. Introduction

Atmospheric gravity waves (GWs) are one of the most important processes in the middle atmosphere (Kim et al., 2003; Fritts and Alexander, 2003). Since the launch of the Upper Atmosphere Research Satellite (UARS) in 1991, the Microwave Limb Sounder (MLS) instrument on board UARS, has provided a wealth of stratospheric GW data quasi-continuously from 1991 to 1997 (Wu and Waters, 1997; Jiang et al., 2003), enabling compilation of multi-year climatologies and investigations of interannual variability and trends (e.g., Jiang et al., 2004b). Most recently, a number of new satellite instruments have been returning vast amounts of new GW data with unprecedented resolution, accuracy and global coverage. Examples include the Advanced Microwave Sounding Unit (AMSU) (Wu, 2004) and the Atmospheric Infrared Sounder (AIRS) on board the Aqua satellite (launched in 2002), the second generation MLS instrument on board Aura (launched in 2004), and a number of current flying low earth orbiters carrying GPS (Global Position System) receivers using radio occultation technology. Multiple-satellite data provide new opportunities for data-model comparisons that can resolve gaps in our knowledge about stratospheric and mesospheric processes.

This study summarizes seasonal climatology of gravity waves observed by UARS MLS in the 1990s, and presents some examples of new GW measurements extracted from AMSU and GPS instruments in the 2000s.

2. UARS MLS observations (1991–1997)

The UARS MLS GW measurements are most sensitive to waves with vertical wavelength >10 km and horizontal wavelength <100 km. A review of the computational procedure of UARS MLS GW radiance variance (including noise removal and recent updates) has been given by Jiang et al. (2004a). The first global

* Corresponding author. Tel.: +1 818 354 7135; fax: +1 818 393 5065.
E-mail address: jonathan@mls.jpl.nasa.gov (J.H. Jiang).

0273-1177/$30 © 2005 COSPAR. Published by Elsevier Ltd. All rights reserved.
doi:10.1016/j.asr.2005.01.099

maps of GW radiance variance derived from UARS MLS data were introduced by Wu and Waters (1996, 1997). Since then, a number of detailed follow-up studies of MLS-observed GWs have been performed, tracing many wave features to tropospheric convection and surface orography through some detailed data-model analyses. For example, Jiang et al. (2004a) modeled MLS measurements of wintertime GW activity in the northern hemisphere using the Mountain Wave Forecast Model (MWFM) in a hindcast mode and with a full limb-track MLS GW visibility function applied to the model output, to mimic observation of these waves from space by MLS. McLandress et al. (2000) and Jiang et al. (2004b) have shown that both the geographical distribution and inter-seasonal variation of subtropical GW variance measured by MLS are closely related to deep convection. These studies also showed that different MLS observation modes (e.g., viewing directions) are sensitive to different wave structures emanating from different sources, due to distinct wind and wave propagation directions at different latitude zones. For example, MLS measurements conducted on north-looking descending (ND) orbits are most sensitive to wintertime orographic GWs at high northern latitudes, while the convection-related subtropical GWs are most prominent in MLS north-looking ascending (NA) and south-looking descending (SD) data. The seasonal and vertical variations of these wave sources are therefore summarized according to various modes of observation spanning different latitude regions.

2.1. Northern high-latitudes

Fig. 1 shows hemispheric maps of the 6-point limb-track ND normalized radiance temperature variances $(T_b'^2/T_b^2)$ at ~33 km averaged for northern winter (December–February, 1994–1997), spring (March–May, 1995–1997), summer (June–August, 1995–1997), and fall (September–November, 1995–1997). Jiang et al. (2004a) have shown that the MLS has greatest sensitivity to mountain waves measured at high latitudes (~50°N–75°N). Their combined data analysis and MLS-filtered MWFM modeling showed that many MLS variance enhancements in the northern hemisphere can be associated with mountain waves forced by flow over specific mountainous terrain. These include mountain ranges in Europe, North America, southeastern Greenland and Iceland.

Due to variation of the stratospheric jet-stream, these orographic waves have a strong reproducible annual cycle, peaking in winter and weakening in other seasons as shown in Fig. 1. Since the MLS variances are related to the GW temperature amplitudes, these measurements can provide critical hemispheric data on mountain wave-induced temperature variability in the high-latitude stratosphere that impacts polar stratospheric cloud (PSC) formation. Such data are critical for refining and constraining the parameterizations for these processes for global chemical transport models (CTMs) of stratospheric ozone evolution (Pierce et al., 2002).

The vertical variation of the wintertime GWs can be seen in Fig. 2, where the MLS variances are mapped at five different altitudes throughout the middle atmo-

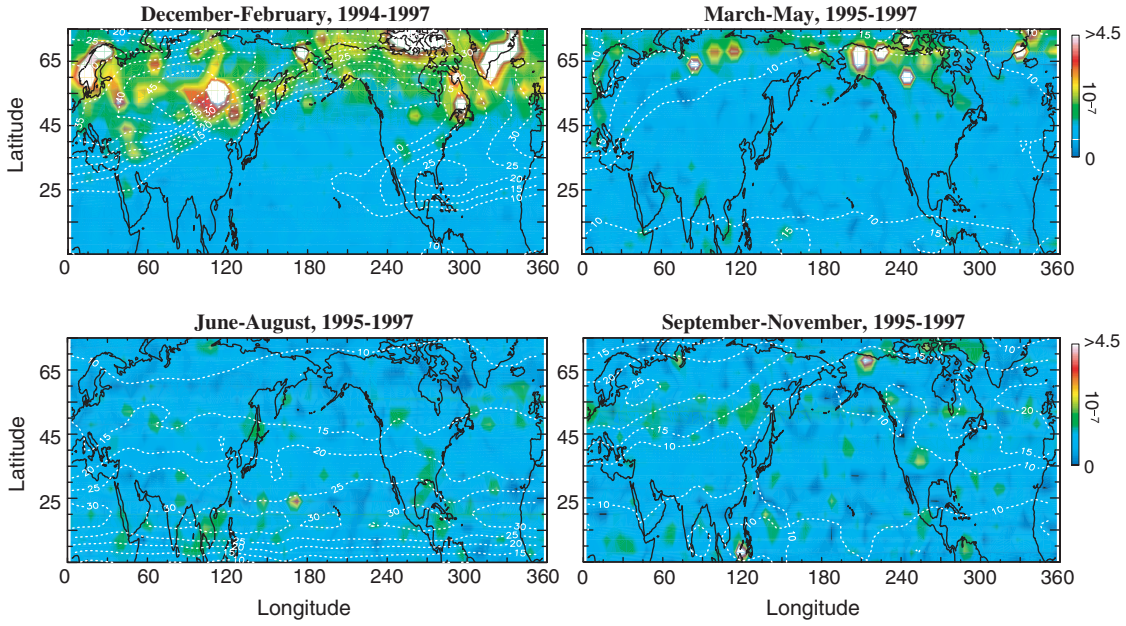

Fig. 1. Seasonal mean fields of normalized radiance temperature variance at 33 km computed from MLS limb-track ND data (as described by Jiang et al. (2004a)). The dotted white contours are UKMO winds at about the same altitudes and averaged over MLS measurement days.

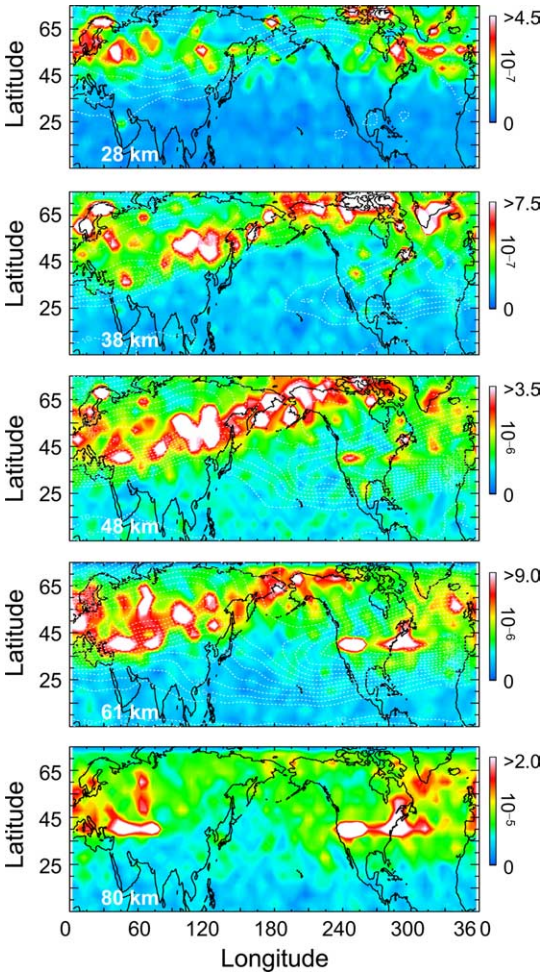

Fig. 2. Maps of wintertime normalized radiance temperature variance at 28–80 km altitudes, computed from MLS limb-track ND data. The dotted white contours below 80 km are UKMO winds. No assimilated wind data are available at 80 km.

sphere (28–80 km). The geographical distributions of GW variance look similar throughout the stratosphere, but undergo some significant changes at the stratopause. For example, the wave variance enhancement over central Eurasia seems to break apart at altitudes above ~60 km, but mid-latitude GW variances across the United States increase above 60 km. The normalized radiance variances can be directly related to GW energy and momentum fluxes. The relative amplitudes of various wave patterns may reflect relative wave dissipation or growth as it enters mesosphere from stratosphere, or may reflect GWs entering/exiting the MLS viewing windows as winds vary with height.

2.2. Sub-tropics

Fig. 3 shows the seasonal maps of subtropical (40°S–40°N) MLS normalized radiance temperature variances averaged for December–February 1991–1994, March–May 1992–1994, June–August, 1992–1994, and September–November, 1992–1994, respectively. As in Jiang et al. (2004b), the MLS 4-point limb-scan NA or SD measurements are used to generate these maps since they are most sensitive to convectively-generated GWs in sub-tropical latitudes.

To see the correlation of the subtropical waves to convective activities, Fig. 4 shows seasonal precipitation maps derived from the NOAA Climate Prediction Center Merged Analysis of Precipitation (CMAP), and averaged for the MLS limb-scan observation days. The CMAP blends station rain gauge observations and five different types of satellite products to estimate global precipitation amounts (Huffman et al., 1997; Xie and Arkin, 1997). Similar to the traditional OLR (outgoing

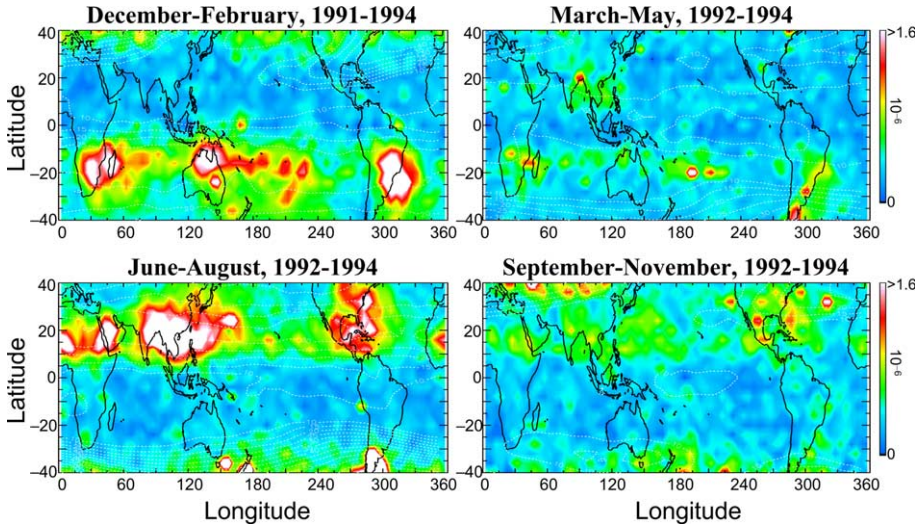

Fig. 3. Seasonal mean fields of MLS normalized radiance temperature variance at 38 km. For December–February 1991–1994 and March–May 1992–1994, the values are computed using measurements from limb-scan NA orbits; for June–August and September–November 1992–1994, limb-scan SD data are used. The dotted white contours are UKMO winds at about same altitudes and averaged over MLS measurement days.

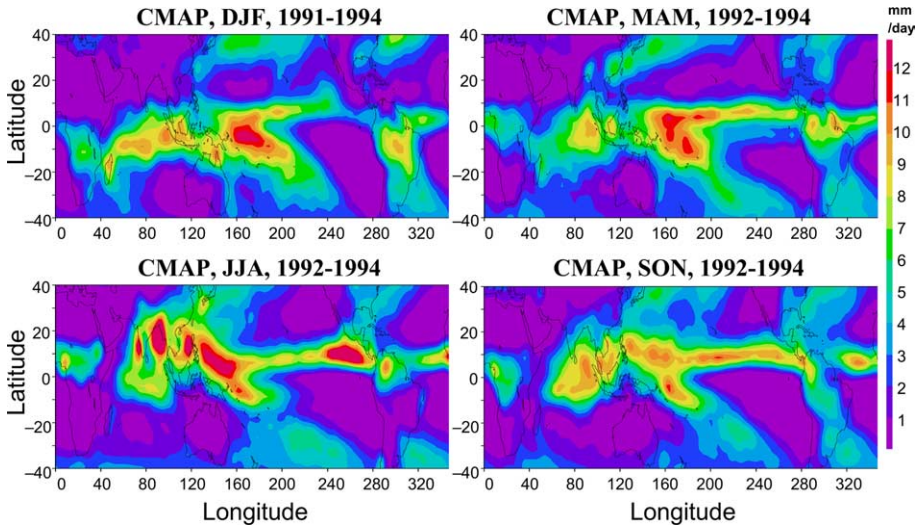

Fig. 4. Seasonal mean precipitation (mm/day) maps derived from the NOAA Climate Prediction Center Merged Analysis of Precipitation (CMAP), and averaged for the same MLS limb-scan observation days.

longwave radiation) data, the CMAP index is a good indicator of deep convection. It shares the common patterns found in OLR data, but tends to include more small-scale details.

Studying Fig. 4, we see that convection events in the tropics appear in all four of the conventional extratropical seasons. Convectively-generated GWs (Fig. 3), however, are predominant in MLS data only in the low latitudes of summer hemispheres, i.e., December–February in southern sub-tropics, and June–August in northern sub-tropics. These are periods when summer monsoon winds enhance local precipitation significantly in the southern and northern subtropics, respectively, yielding ''wet seasons''. Wind contours in Fig. 3 also show that these subtropical variance enhancements occur where mean winds are largest. Studies by Jiang et al. (2004b) found that most convectively-generated GWs can be seen by MLS in the stratosphere only when the background winds are westward, and exceeding ~20 m/s (see Fig. 8 of Jiang et al. (2004b)). This criterion is met only in the summer subtropics. Another noticeable phenomenon is the asymmetries between the southern summer (top-left) and northern summer (lower-left) convectively-generated waves seen by MLS. Comparing variances in Fig. 3 to the CMAP indices in Fig. 4, we see that the centers of enhanced variances are often shifted ~10° in latitude poleward from of the convection centers. Jiang et al. (2004b) suggested this observed poleward shift may result from the background wind filtering of the GW propagating into the stratosphere and is also likely related to the MLS GW visibility function, since local winds are weaker over the convection centers. However, further modeling effort is needed to fully understand this phenomenon.

The vertical variations of the December–February and June–August summertime subtropical wave fields in Fig. 4 are shown in Fig. 5, where the normalized radiance variances are mapped at five different altitudes (28–80 km). The wave activity patterns for both the southern (left-column) and northern (right-column) summer monsoon seasons are mostly maintained throughout the stratosphere, although some slight poleward shifts are noticeable between 28 and 33 km. This suggests fast waves that propagate into the mesosphere without extensive lateral propagation, consistent with current theories and modeling studies (e.g., Horinouchi et al., 2002). However, the patterns undergo significant changes above the stratopause at 61 and 80 km, with the emergence of high latitude wave patterns. The much broader vertical width of the channel 7 (~80 km) weighting function (Wu and Waters, 1997) may also play a significant role in modifying geographical variance distributions.

2.3. Southern high-latitudes

Seasonal MLS normalized radiance variance maps at ~33 km in the extratropical southern hemisphere (Fig. 6) reveal enhancements at high southern latitudes. Enhancements start to appear in May, peak in southern winter (June–August) and continue into the southern spring (September–November). The large variance enhancement over the southern tip of the Andes Mountains was analyzed previously using combined MWFM modeling and MLS data analysis (Jiang et al., 2002). Other variances peaks also occur, such as a longitudinal broad variance enhancement over the Southern Ocean that follows the polar vortex edge region where zonal winds are strong. Thus, to first order these enhancements are consistent with dilated GW vertical wavelengths in strong winds which make all GWs here more visible to the MLS instrument. Some of the

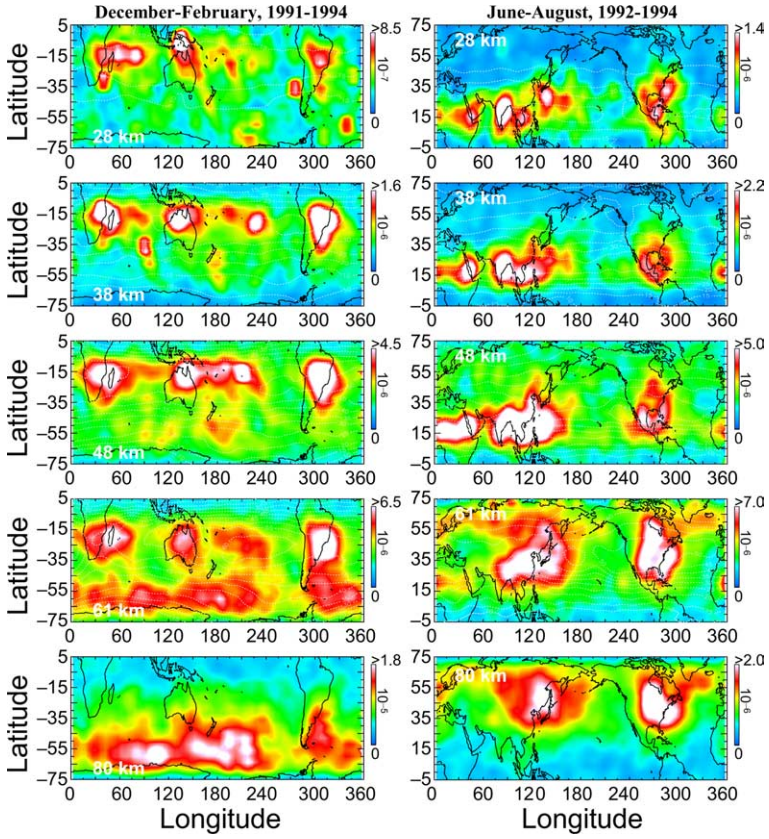

Fig. 5. Maps of normalized radiance temperature variance at 28, 38, 48, 61 and 80 km altitudes. The data December–February (left) are computed using MLS limb-scan SD measurements; for the June–August maps (right), MLS limb-scan NA data are used. The dotted white contours below 80 km are UKMO winds at about same altitudes and averaged over MLS measurement days. No assimilated wind data are available at 80 km.

variance enhancements seem to related to underlying orography, such as those over the Palmer Peninsula (300°E, 65°S) and the coastal Transantarctic Mountains near McMurdo Sound (~165°E, 70–75°S). However, preliminary modeling using MWFM (Fig. 7) reveals that much of these MLS wave patterns occurs well away from predicted orographic GWs and thus many variance enhancements are likely nonorographic in origin. For example, intense evolving weather phenomena such as the strong baroclinic storm systems develop along

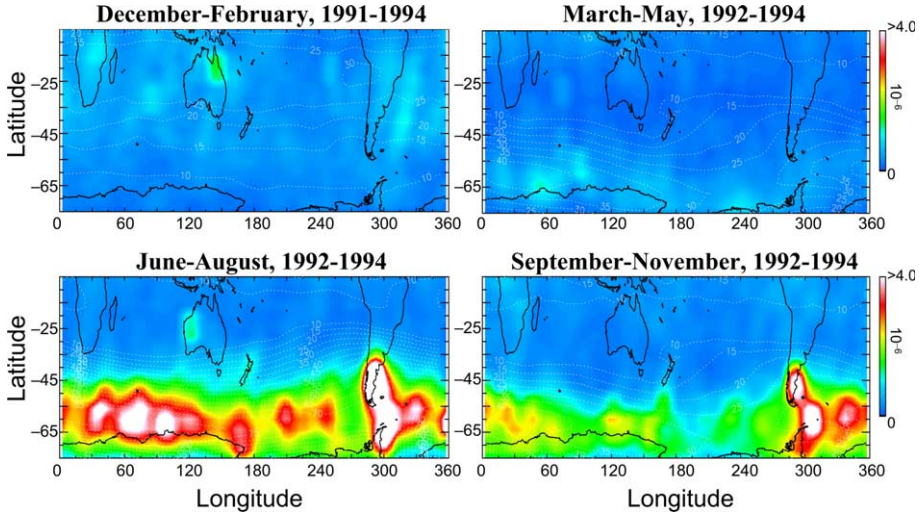

Fig. 6. Seasonal mean fields of normalized radiance temperature variance at 33 km computed from MLS limb-scan SA measurements. The dotted white contours are UKMO winds at about same altitudes and averaged over MLS measurement days.

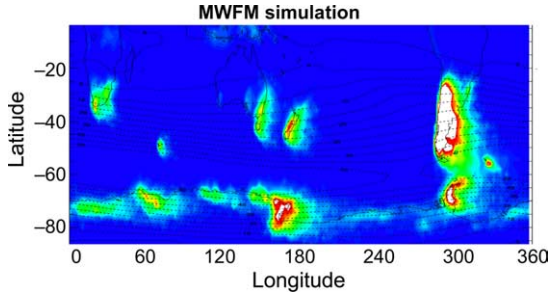

Fig. 7. MWFM simulated 5 mb orographic waves (as temperature perturbation) averaged over MLS limb-scan days (June–August 1992–1994). No observational filter was applied in this simulation. Maximum contour value is 5 K.

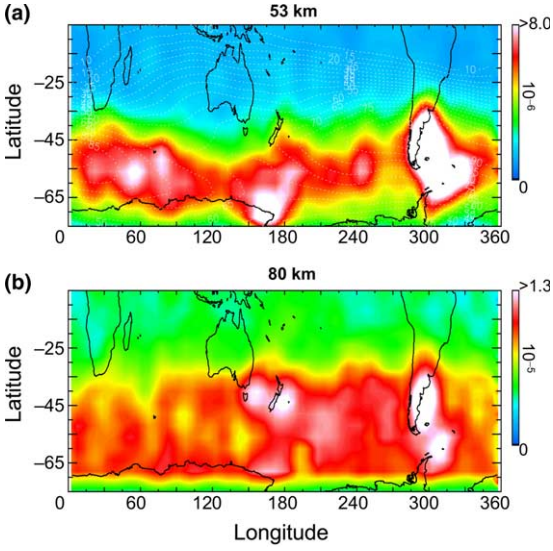

Fig. 8. June–August 1992–1994 mean MLS normalized limb-scan SA radiance variance map for 53 km (a) and 80 km (b).

this "roaring forties" region of the Southern Ocean and can radiate gravity waves from jet-stream instabilities (e.g., O'Sullivan and Dunkerton, 1995; Guest et al., 2000).

As altitude increases, these GW enhancements increase in magnitude but maintain almost the same geographical distribution until ~53 km (Fig. 8(a)), where the waves along the Antarctic edge over the Southern Ocean start to level off (Fig. 8(b)). The orographic GW variances, such as those over the southern Andes and New Zealand regions, however, seem to maintain their strength well into the mesosphere at 80 km.

3. Other satellite measurements (2001-present)

A suite of new satellite instruments recently launched into orbit are beginning to return a wealth of radiance and/or temperature data containing GW information with high resolution, accuracy and global coverage. This offers researchers an unprecedented, long-term global stratospheric and mesospheric gravity wave product. Some examples of these new datasets are briefly introduced below.

3.1. GPS radio occultation

GPS radio occultation technology is developing into a powerful tool for continuously monitoring the Earth's atmosphere. The GPS constellation consists of about 30 satellites that are distributed in circular orbits at ~20,000 km altitude. Recently launched German CHAMP and Argentinean SAC-C low-orbit satellites each carry a new-generation GPS receiver, the "Black-Jack." These receivers have been collecting occultation data to retrieve profiles of atmospheric refractivity, temperature, pressure, and water vapor since mid-2001 (Hajj et al., 2002). As demonstrated by Tsuda et al. (2000) using earlier GPS/MET data, GPS occultation temperatures can be used to extract gravity wave information. As an example, Fig. 9 displays the temperature variances derived from the GPS/CHAMP measurements (left) and water vapor pressure obtained from NCEP reanalyses (right). The temperature variance data are

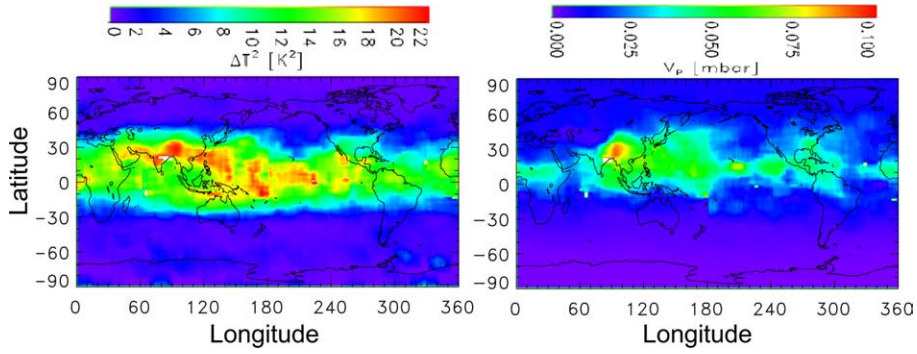

Fig. 9. Mean temperature variances of gravity waves derived from GPS/CHAMP measurements (left) averaged for July–September 2002 between 15 and 25 km height. The right panel is the NCEP water vapor pressure at ~10 km and interpolated for time and place of the given occultation event.

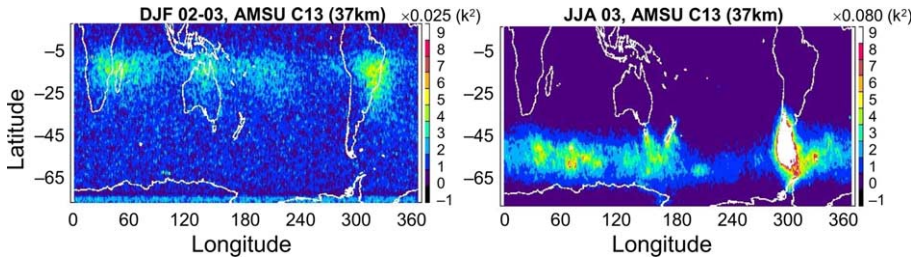

Fig. 10. Mean seasonal gravity wave variance maps of the southern hemisphere derived from AMSU-A measurements for December–February 2002–2003 (left) and June–August 2003 (right). The altitude is ~37 km.

averaged for the period of July–September 2002 within the height interval of 15–25 km. During that period the GPS receiver onboard the CHAMP satellite collected ~10,000 temperature profiles over the globe. The GW activity superimposed upon a temperature profile is estimated by averaging the small-wavelength variance of the vertical temperature fluctuations between 15 and 25 km. The temperature fluctuations are extracted from the temperature profiles by means of a non-recursive digital filter (Kaiser filter) having a band pass of 10–15 km. The variance values are arranged as a function of geographic longitude and latitude of the occultation events, and computed with a boxcar average having a box-size of 15° longitude by 10° latitude and moving with a step of 1°. From this variance map (left panel) and the correlated NCEP water vapor reanalysis field (right panel), one can see two regions where GW variance and moisture correlate well: one around the Bangladesh region (possibly related to the Indian monsoon in summer of 2002), and another in the equatorial zone over the Western Pacific. As a measure of deep water vapor convection, the averaged water vapor pressure around 10 km is depicted in the right panel of Fig. 9. These GW active regions have come under increasing scrutiny in recent years as a possible major player in the water vapor budget near the tropopause and lower stratosphere (e.g., Jensen et al., 2001). A recent study by Wu et al., this issue suggests that due to the vertical and horizontal resolutions, GPS GW measurements are mostly limited to waves of short vertical (<10 km) and long horizontal (>200 km) wavelengths.

3.2. AMSU observation

A variance analysis technique has recently been developed by Wu (2004) to extract gravity wave induced temperature fluctuations from the AMSU radiance measurements on board the Aqua satellite. The algorithm has produced reliable gravity wave variance maps with very high resolution of 0.5° by 0.5° longitude by latitude grid, enabling geolocation of small-scale regional wave features. Shown in Fig. 10 are AMSU-A seasonal mean radiance variance maps for December–February 2002–2003 (left) and June–August 2003 (right) at ~37 km. These maps have many similarities with the corresponding UARS MLS seasonal maps (see, e.g., Figs. 3 and 6), including the three convection centers in southern summer sub-tropics, their poleward shift, and the large wave enhancements over the southern Andes and along the Antarctic edge over the Southern Ocean. The AMSU GW measurements are mostly sensitive to waves having vertical wavelength >10 km and horizontal wavelength of 50–150 km (Wu et al., this issue).

4. Concluding remarks

We have presented a summary of seasonal global climatologies of middle atmospheric GWs derived from UARS MLS measurements and have demonstrated examples of some newer GW data derived from more recent GPS and AMSU observations. Recent GW measurements from other satellite instruments can also be found in a number of review papers (e.g., Wu et al., this issue; Fritts and Alexander, 2003). In the past, conventional gravity wave observations have mostly been conducted from ground-based sounders (e.g., lidar, radar), rockets, balloons, and aircraft. Although these observations have given us important information on gravity wave properties, they provide only a local picture. This complicates the analysis of GWs: for example, waves can propagate both vertically and horizontally over long horizontal distances, and only a small portion of the wave's full life cycle may be measured by a ground-based vertical profiling instrument as the wave propagates obliquely across the instrument's vertical field of view. Thus, truly global measurements of GWs at a range of stratospheric and mesospheric altitudes from high-resolution satellite instruments are especially valuable for understanding the full three-dimensional picture, such as the intensity and geographical variability of the tropospheric sources of GWs. Nonetheless, these space-based observations require support by appropriate global modeling of anticipated wave signatures which account for the observational filtering properties of the GW detection, to permit effective interpretation of the measurements (e.g., Jiang et al. (2004a)). Such data-model studies will provide and validate the most

complete long-term global data on gravity waves in the middle atmosphere, and help resolve gaps in our knowledge about stratospheric and mesospheric processes that are crucial to the advancement of atmospheric science.

Acknowledgments

The first author (J.H.J.) like to thank Prof. T. Nakamura and Dr. M.J. Taylor for invitation to present this paper at 35th COSPAR Scientific Assembly in Paris, and for valuable comments and suggestions. This study was supported by the Jet Propulsion Laboratory, California Institute of Technology, under contract with NASA. S.D.E.'s work was partially supported by The Office of Naval Research and by NASA's Geospace Sciences Program. The authors also appreciate the support of the University of Hawaii of USA, and the National Institute of Information and Communications Technology of Japan.

References

Fritts, D.C., Alexander, M.J. Gravity wave dynamics and effects in the middle atmosphere. Rev. Geophys. 41 (1), 1003, 2003.

Guest, F.M., Reeder, M.J., Marks, C.J., Karoly, D.J. Inertia-gravity waves observed in the lower stratosphere over Macquarie Island. J. Atmos. Sci. 57, 737–752, 2000.

Hajj, G.A., Kursinski, E.R., Romans, L.J., Bertiger, W.I., Leroy, S.S. A technical description of atmospheric sounding by GPS occultation. J. Atmos. Solar-Terr. Phys. 64, 451–469, 2002.

Horinouchi, T., Nakamura, T., Kosaka, J. Convectively generated mesoscale gravity waves simulated throughout the middle atmosphere. Geophys. Res. Lett. 29, 2007, 2002.

Huffman, G.J., Adler, R.F., Arkin, P., Chang, A., Ferraro, R., Gruber, A., Janowiak, J., McNab, A., Rudolf, B., Schneider, U. The Global Precipitation Climatology Project (GPCP) combined precipitation dataset. Bull. Am. Meteor. Soc. 78 (1), 5–20, 1997.

Jensen, E.J., Pfister, L., Ackerman, A.S., Tabazadeh, A., Toon, O.B. A conceptual model of the dehydration of air due to freeze-drying by thin, laminar cirrus rising slowly across the tropical tropopause. J. Geophys. Res. 106, 17, 2001, 237–17, 252.

Jiang, J.H., Wu, D.L., Eckermann, S.D., Ma, J. Mountain waves in the middle atmosphere: microwave limb sounder observations and analyses. Adv. Space Res. 32, 801–806, 2003.

Jiang, J.H., Wu, D.L., Eckermann, S.D. Upper Atmosphere Research Satellite (UARS) MLS observation of mountain waves over the Andes. J. Geophys. Res. 107, D22, 2002.

Jiang, J.H., Eckermann, S.D., Wu, D.L., Ma, J., A search for mountain waves in MLS stratospheric limb radiances from the winter Northern hemisphere: data analysis and global mountain wave modeling, J. Geophys. Res. 109 (D3), D03107, 2004a.

Jiang, J.H, Wang, B., Goya, K., Hocke, K., Eckermann, S.D., Ma, J., Wu, D.L., Read, W.G. Geographical distribution and interseasonal variability of tropical deep convection: UARS MLS observations and analyses. J. Geophys. Res. 109 (D3), D03111, 2004b.

Kim, Y.-J., Eckermann, S.D., Chun, H.-Y. An overview of the past, present and future of gravity-wave drag parametrization for numerical climate and weather prediction models. Atmos. Ocean 41, 65–98, 2003.

McLandress, C., Alexander, M.J., Wu, D.L. Microwave limb sounder observations of gravity waves in the stratosphere: a climatology and interpretation. J. Geophys. Res. 105, 11947–11967, 2000.

O'Sullivan, D., Dunkerton, T.J. Generation of inertia-gravity waves in a simulated life cycle of baroclinic instability. J. Atmos. Sci. 52, 3695–3716, 1995.

Pierce, R.B. et al. Large-scale chemical evolution of the Arctic vortex during the 1999/2000 winter: HALOE/POAM III Lagrangian photochemical modeling for the SAGE III–Ozone Loss and Validation Experiment (SOLVE) campaign. J. Geophys. Res. 107, 8317, 2002.

Tsuda, Nishida, T.M, Rocken, C. A global morphology of gravity wave activity in the stratosphere revealed by the GPS occultation data (GPS/MET). J. Geophys. Res. 105, 7257–7274, 2000.

Wu, D.L., Waters, J.W. Gravity-wave-scale temperature fluctuations seen by the UARS MLS. Geophys. Res. Lett. 23, 3289–3292, 1996.

Wu, D.L., Waters, J.W. Observations of gravity waves with the UARS Microwave Limb Sounder, Gravity Wave Processes. NATO ASI Series I: Global Environment Change 50, 103–120, 1997.

Wu, D.L. Mesoscale gravity wave variances from AMSU-A Radiances. Geophys. Res. Lett. 28 (No. 12), 2004.

Wu, D.L., Preusse, P., Eckermann, S.D., Jiang, J.H., De la T. Juarez, M., Coy, L., Wang, D.Y., Remote sounding of atmospheric gravity waves with satellite limb and nadir techniques, Adv. Space Res., this issue.

Xie, P., Arkin, P.A. Global precipitation: A 17-year monthly analysis based on gauge observations, satellite estimates, and numerical model outputs. Bull. Am. Meteor. Soc. 78 (11), 2539–2558, 1997.